

## **Depth Resolved Measurement of the 3D Residual Stress State in Surface Engineered Aluminium by Synchrotron Diffraction**

ASQUITH, David <<http://orcid.org/0000-0002-0724-7415>>, HUGHES, Darren, HATTINGH, Danie, JAMES, Neil, JOHN, Yates and ALEKSEY, Yerokhin

Available from Sheffield Hallam University Research Archive (SHURA) at:

<http://shura.shu.ac.uk/11293/>

---

This document is the author deposited version. You are advised to consult the publisher's version if you wish to cite from it.

### **Published version**

ASQUITH, David, HUGHES, Darren, HATTINGH, Danie, JAMES, Neil, JOHN, Yates and ALEKSEY, Yerokhin (2013). Depth Resolved Measurement of the 3D Residual Stress State in Surface Engineered Aluminium by Synchrotron Diffraction. In: SHIH, Kaimin, (ed.) X-Ray Diffraction : Structure, Principles and Applications. Materials Science and Technologies . Nova Science.

---

### **Copyright and re-use policy**

See <http://shura.shu.ac.uk/information.html>

*Chapter*

**DEPTH RESOLVED MEASUREMENT OF THE 3D  
RESIDUAL STRESS STATE IN SURFACE ENGINEERED  
ALUMINIUM BY SYNCHROTRON DIFFRACTION**

***DT Asquith<sup>1</sup>, DJ Hughes<sup>2</sup>, DG Hattingh<sup>3</sup>,  
MN James,<sup>4,3</sup> JR Yates<sup>5</sup> and A Yerokhin<sup>\*6</sup>***

<sup>1</sup>Sheffield-Hallam University, UK.

<sup>2</sup>ILL, Grenoble, France

<sup>3</sup>Nelson Mandela Metropolitan University, SA

<sup>4</sup>University of Plymouth, UK

<sup>5</sup>University of Manchester, UK

<sup>6</sup>University of Sheffield, UK

**ABSTRACT**

Evaluation of the complex three dimensional residual stress states in manufactured components is an important part of assessing the durability of safety critical components. Many experimental techniques have been used in attempts to quantify residual stresses. Few are capable of resolving the full stress tensor in engineering components. In this work a method for measuring the three dimensional residual stress state has been proposed and demonstrated experimentally. Strains have been measured in machined and shot-peened aerospace aluminium alloy specimens by X-ray diffraction in the ESRF Synchrotron Facility. Data from four orientations have been collected so that both the magnitude and direction of the principal stresses can be determined. The problems of gauge volume size and specimen orientation relative to the beam were addressed and resolved. Effects of the specimen location relative to the beam, translation hardware repeatability, beam slits and spectrum acquisition time are discussed. The differences observed between a 2D and 3D evaluation of the same data suggest that measurement techniques using only in-plane data can be misleading so care should be taken when using such data to guide simulations.

---

\* Corresponding Author. Tel: +44-11422-25510; Fax: +44-11422-25943; E-mail: A.Yerokhin@sheffield.ac.uk

## 1. INTRODUCTION

Almost all manufacturing processes, from the casting of a billet to the final surface finishing of a component, result in residual stresses being locked into the product. These residual stresses are likely to vary in magnitude and orientation throughout the structure. They will interact with intrinsic defects in the material, with the geometric features of the component and with the stresses generated by the service loads. Beneficial compressive residual stresses, such as those introduced by shot-peening will enhance the integrity of the structure, but tensile stresses can contribute to premature failure by fracture or fatigue.

The measurement of residual stresses has been the subject of extensive research over a period of many years. Several reviews and reports on the sources and measurement of residual stresses have been published, including those by Withers and Bhadesia [1,2] and the NPL [3]. Reimers, et al [4], Pyzalla [5] and James, et al [6] have described the use and advantages of hard X-ray synchrotron radiation in measuring the residual stress state of engineering features, such as friction stir welds. Frequently, when collecting diffraction data one assumes prior knowledge of the principal stress directions [7, 8]. Often this is taken to be the parallel and perpendicular to the rolling direction of a plate. This may well be a reasonable assumption in some circumstances, but it cannot be a universal truth. The difficulty in testing this assumption is in acquiring data from a sufficient number of directions to resolve both the magnitude and direction of the strains.

It is possible with the use of high power x-ray (synchrotron) radiation to penetrate much greater distances in many structural materials than with conventional lab sources; approximately 10mm in aluminium. This enables the measurement of strains at a number of points throughout the surface and bulk of a specimen without any destructive procedures. Consequently this allows the analysis of a number of directions of strain to be made and retain the sample for further work. By careful orientation of the illuminated gauge volume employed in the strain measurements, it is possible to achieve similar spatial resolution for all directions of strain measured, thus providing a set of data which can be reasonably combined into the three principal strains. This work describes one approach for measuring sufficient directions of strain to calculate a three dimensional stress state. As an example data from an experiment involving shot-peened aluminium using measurements made at the ESRF, Grenoble, France is presented. Furthermore it shows that the 3D profile obtained provides significantly more data with some subtle differences to that typically obtained through a 2D profile, in plane evaluation. Although demonstrated with cold-worked aluminium the technique is equally applicable to any metallic material within the limitations of the x-ray source attenuation.

## EXPERIMENTAL TECHNIQUE

### 2.1. $\theta$ - $2\theta$ Strain Measurements

While several approaches to evaluating strain using diffraction exist, this method utilises ~~a the~~ phenomenon ~~of the~~ Bragg peak shift with applied elastic strain, which is evaluated in a  $\theta$ - $2\theta$  configuration by comparison with a strain free lattice parameter. This technique is

briefly described here. When the diffraction geometry satisfies the Braggs' condition whereby:

$$n\lambda = 2d \sin \theta$$

Constructive interference occurs producing an intense peak. The position of this peak in terms of the diffraction angle,  $\theta$ , varies with a change in the crystallographic lattice spacing,  $d$ , and the diffracting wavelength,  $\lambda$ . Evaluating a particular  $hkl$  peak with a fixed wavelength of x-rays provides information of the particular lattice spacing,  $d$ . If an elastic strain is applied to the material, its  $d$  value changes accordingly. Two peaks for a strained and strain free material are shown in Figure 1.

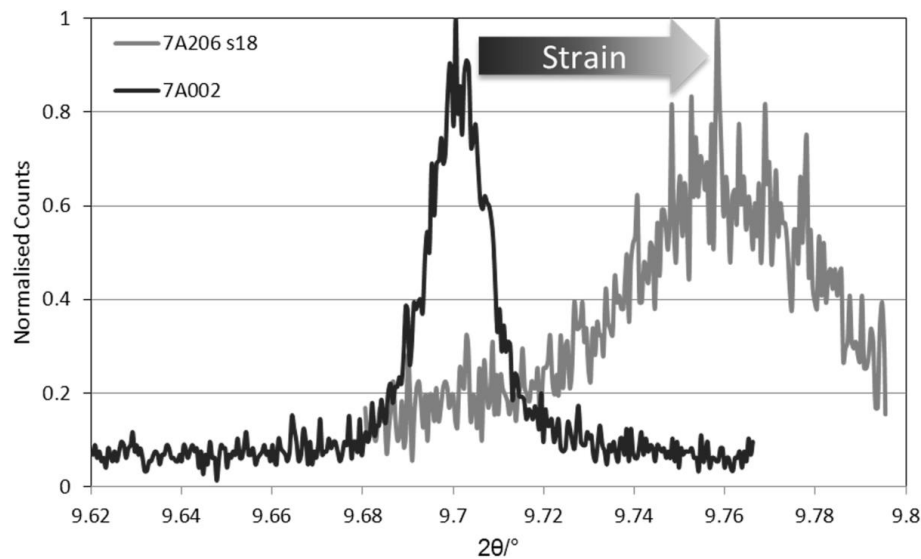


Figure 1. Peak shift due to elastic strain in an aluminium alloy.

Using a source of highly collimated x-rays such as those produced in a synchrotron allows the definition of a small diffracted gauge volume, as the detected beam is effectively coherent due to the acceptance crystals we can accurately define both the location and direction of measured strain as a function of the experimental parameters. Due to the polycrystalline nature of metallic materials it is possible to make measurements on the same  $hkl$  plane in several physical orientations of the specimen which is necessary to calculate a full strain tensor.

Due to the dependence of the crystallographic spacing on materials properties, such as those modified by alloying and processing, it is necessary to make an evaluation of a representative unstrained lattice parameter. One effective approach for doing this is described by Hughes, et al [9] and involves relaxing the strain without extensively modifying the microstructure by creating small comb teeth in a representative specimen and averaging the  $d$  measurements across several teeth.

## 2.2. Specimen Orientations for Individual Strain Measurements

Firstly, it must be noted that residual stresses are evaluated from measurements of residual strain. In general, measurements in at least five different directions would be required, if the full three dimensional stress state were to be evaluated without *a priori* knowledge, or assumption, of the principal directions. This can be reduced to four individual directions provided three of these can be considered to lie in a plane defined by two of the principal directions. This allows us to assume that the third principal direction is perpendicular to the defined plane and can be measured individually as a fourth direction. In the experiment presented here the process of shot-peening the specimen surface creates conditions which satisfy the above assumption thereby simplifying the experimental work.

The four required strain directions are identified here as  $\epsilon_a$ ,  $\epsilon_b$ ,  $\epsilon_c$  and  $\epsilon_d$ , they are demonstrated in Figure 2 relative to the specimen shown geometry. Having obtained a suitable measure of strains for a given point in the material we must then evaluate the principal directions of strain, this can be done simply by applying Mohr's circle.

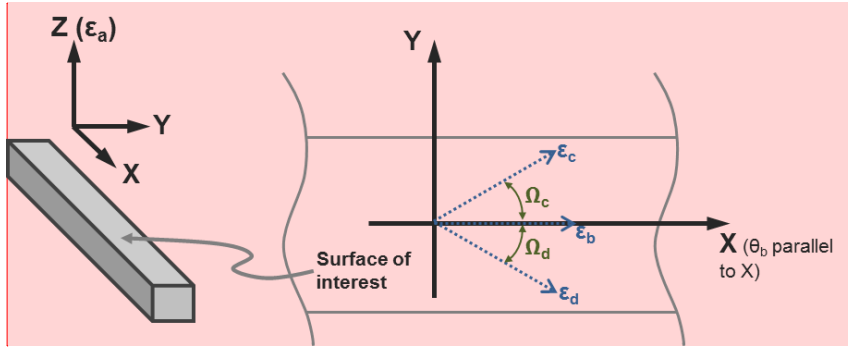


Figure 2. Measured strain directions relative to specimen, the remaining direction of strain ( $\epsilon_a$ ) is coordinate with Z in the left-hand diagram, and it corresponds to one of the principal directions.

The experimental challenge is to orientate the specimen with respect to the beam in such a way that sufficient sets of data are obtained. Two characteristics of the beam make this difficult. The first is the attenuation of the beam as it passes through the aluminium. This becomes critical when exploring the sub-surface layers, and also when there is a shallow angle of incidence between the beam and the specimen. As the diffracted portion of the beam approaches the axis of the longer specimen dimension, the length of attenuating material the beam must pass through increases thus reducing flux at the detector, and increasing the necessary count time.

Having defined a plane in the specimen surface in which three of the required directions lie also allows one setup to be used to measure these. It is necessary to rotate the specimens about the experimental  $\theta$  axis, normal to the plane, but this facility is provided for as a basic diffractometer requirement. This setup utilises gauge volume  $G_{b,c,d}$  and is, in this case, a transmission arrangement. The first measured direction,  $\epsilon_b$ , is measured nominally in the rolling direction (X) and requires the specimen to be orientated at the diffraction angle  $\theta$  to the beam. The measured directions  $\epsilon_b$  and  $\epsilon_c$  are obtained by rotating the specimen toward and

**Comment [DA1]:** I've updated this figure it had none of the annotation on it in the proof... it also takes up less room now.

away from the beam relative to  $\varepsilon_b$ . In this case an angle of  $30^\circ$  was used as a compromise between attenuation and error in resolved strain. Figure 3 shows this relative to the specimen geometry and beam with an image of the actual setup for clarity. The fourth direction, (Z) perpendicular to this defined plane, requires the specimens to be rotated about the axis of the beam and so necessitates a different experimental setup using gauge volume  $G_d$  in reflection. These measurements are inherently slower since the gauge volume is slightly smaller and as such longer count times are required. The setup used for obtaining  $\varepsilon_d$  is less easily represented with a 2D schematic, Figure 4 shows a 3D visualisation with a photograph for comparison with Figure 3.

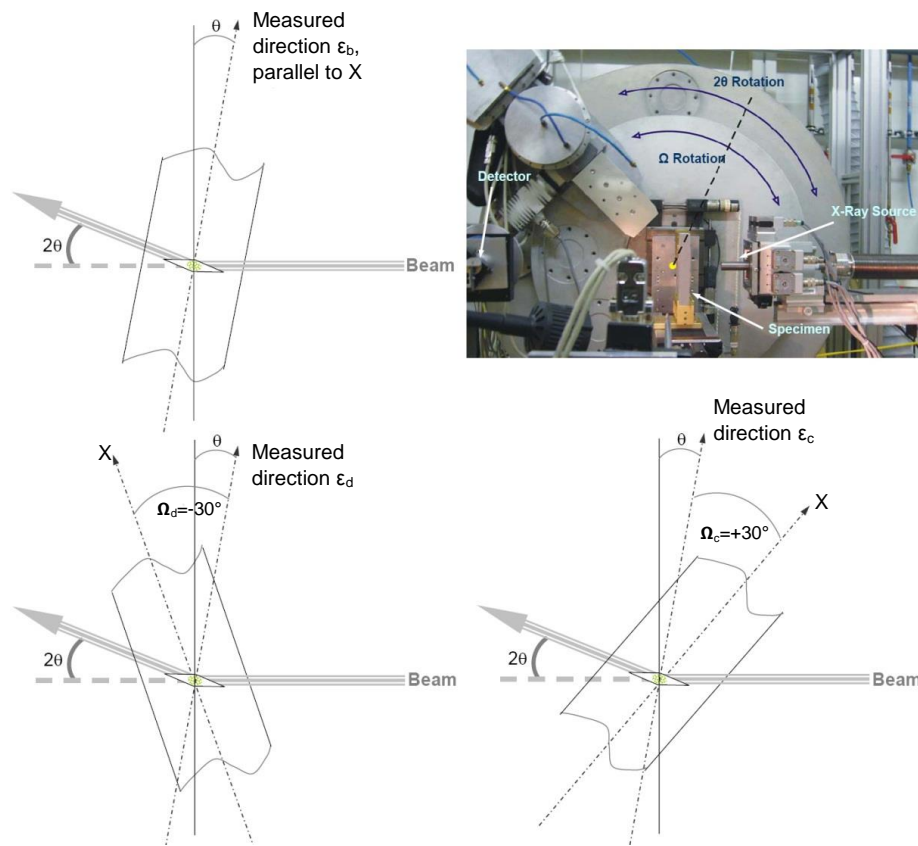


Figure 3. Specimen orientations for in-plane strain measurements (transmission) and actual setup on experimental beamline ID31.

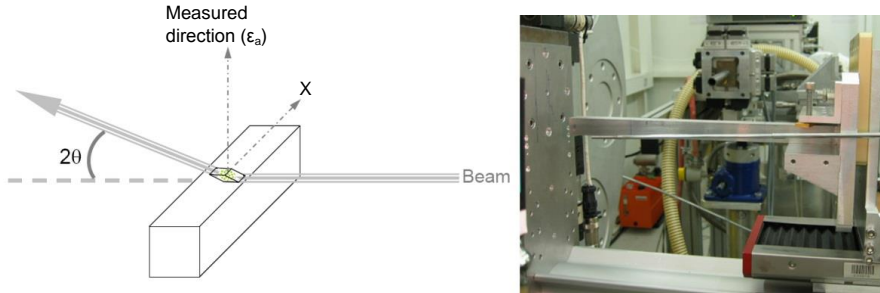


Figure 4. Specimen orientation for out-of-plane strain measurement (reflection) and setup on experimental beamline. Note that the diagram observes from a different angle to the photograph, in which the arrow denotes the beam direction.

### 2.3. Gauge Volumes for in-Plane and Out-of-Plane Measurements

The second important consideration is the ‘gauge volume’, that is, the size and shape of the illuminated volume of material causing the diffraction of the beam. The spatial resolution of the strain gradient with respect to depth depends, amongst other factors, on the size and shape of the gauge volume. Changing the gauge volume according to the desired resolution and orientation is the key to be able to collect sufficient data to resolve the three dimensionality of the stress state. By choosing gauge volume dimensions that are small in the stepping direction spatial resolution can be maximised. To provide a good average of the strain state present it is necessary to maximise other dimensions, thereby including a sufficient number of individual grains in the diffracting orientation. This also reduces the count time required for each data point. Since strains are to be measured in different directions and using both transmission and reflection, it is unreasonable to assume a single shape of gauge volume will suffice for all measurements. In this work two different arrangements were used to optimise the spatial resolution for different measurement directions. By designing the gauge volumes to provide uniform resolution in the step direction for each direction of strain, it is possible to correlate individual data points allowing the combination of individual measurements to evaluate principal directions and then subsequently the stresses.

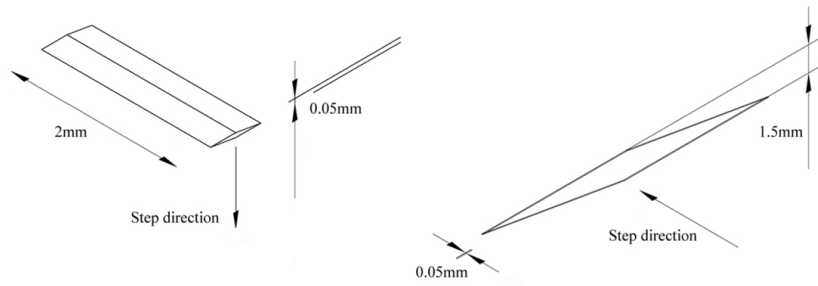


Figure 5. Gauge volume shapes (not to same scale), volume  $G_a$  is on the left,  $G_{b,c,d}$  the right.

Figure 5 shows the shapes of both gauge volumes used in the following case study. In practice the gauge volumes are defined by limiting the horizontal and vertical dimension of the beam, it is absolutely critical to the success of such experiments that this is both accurate and repeatable with well-engineered beam slits. Having established a limited gauge volume from which to diffract, the specimen is then orientated relative to this such that the desired direction of strain can be evaluated; it can then be stepped relative to the gauge volume to obtain strain variation with respect to the step direction. In all cases the step direction is parallel to the shortest dimension, thus providing highest resolution.

### 3. CASE STUDY

For this chapter a case study is taken from research presented by Asquith [10], and specimens were produced from the structural aluminium alloy 7050-T7451. Plates of 20mm thickness were sectioned and machined into specimens measuring 20×20×50mm as shown in Figure 6. Specimens were shot-peened at the University of Sheffield using a Tealgate Precifeed system, the peened surface is identified in Figure 5 as a hatched surface. Parameters were taken from prior work on the optimisation of the shot-peening process undertaken at the University of Sheffield [11].

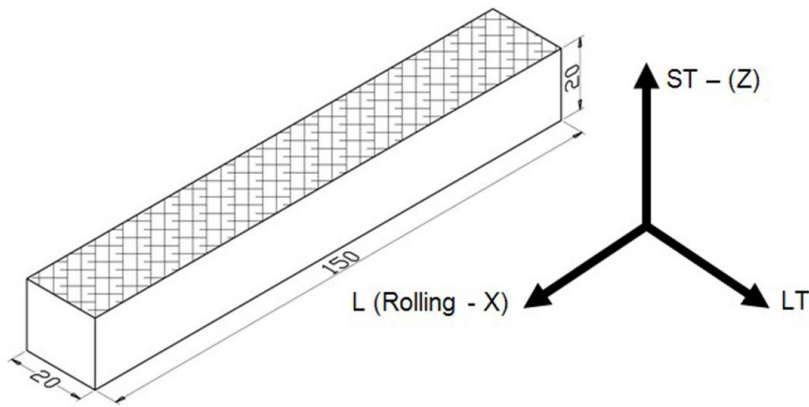


Figure 6. Tested aluminium alloy plate with dimensions in mm (surface of interest hatched).

Residual stresses were evaluated by high resolution synchrotron diffraction at the ESRF, Grenoble (beam-line ID31). The strains were measured using a highly collimated monochromatic hard X-ray beam ( $E=60\text{keV}$ ,  $\lambda=0.206\text{nm}$ ). The measurements were taken starting from the surface with an increment size of  $20\mu\text{m}$  to a depth of  $0.5\text{mm}$  and then in  $50\mu\text{m}$  increments to  $1\text{mm}$ . For each depth increment, the strain was measured in four different directions (three in the plane of, and one normal to, the specimen surface) allowing principal strains to be resolved using Mohr's circle and subsequently evaluated the three principal residual stresses using Hooke's law, as discussed in section 2. The two principal



directions in the surface plane were assumed to be orthogonal. The changes in residual elastic strain were evaluated using the Braggs' equation:

$$\varepsilon = \frac{\theta - \theta_0}{\tan \theta_0} = \frac{d - d_0}{d_0}$$

where  $\theta_0$  and  $d_0 = 0.1213346 \pm 0.000264 \text{ nm}$  correspond to the unstrained Al (311) peak centre and lattice spacing respectively, obtained using a sample that had been machined into a comb profile with  $\approx 1 \text{ mm}^2$  teeth in order to relieve the residual stress.

## 4. RESULTS

### 4.1. Measured Strains

Figure 7 below shows strain measured in four directions with respect to depth in the specimen surface. The spatial resolution required throughout the depth is not uniform, and more detail is needed in the near surface where the strain profile changes more rapidly. Toward the centre of the specimen the profile is less altered by the shot-peening. Therefore, the gradient is lower and less frequent measurements are required to characterise the strain field. As may be expected, the in-plane measurements show similar behaviour and are typical of the residual strain profile commonly presented for shot-peened aluminium. Of particular interest though is the out of plane strain. This is considered in some cases to be zero, particularly if a state of plane stress is assumed, but can clearly be seen here to vary significantly with depth and exhibits substantial tension in the near surface.

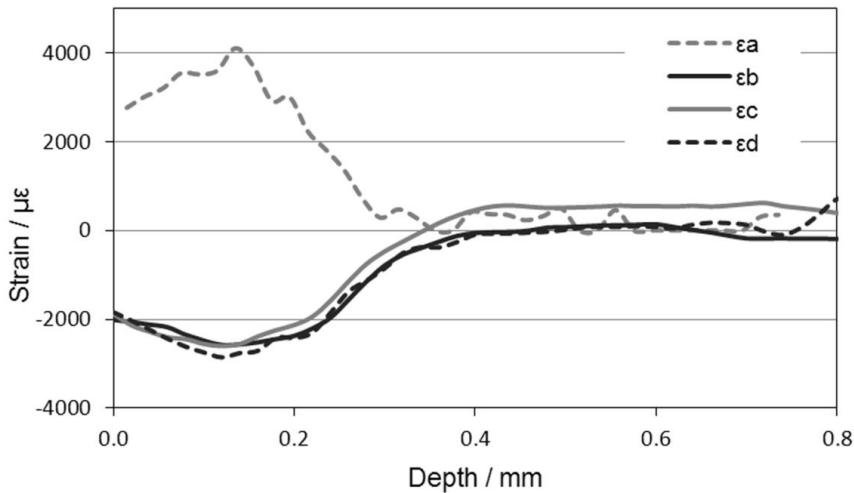


Figure 7. Strains measured in shot-peened AA7050 in different directions with increasing depth in the specimen.

#### 4.1. Evaluating Principal Strains

Assuming that two of the three principal strains lie in the plane of the surface, we can define the normal direction as a third principal. It then remains to translate the three measured in-plane directions to the principal directions. This process requires two stages; firstly, the three measured in-plane strains must be translated to two arbitrary but orthogonal axes. Secondly the principal strains and their direction relative to the specimen geometry can be obtained from the orthogonal strains by applying Mohr's circle. Translating three strains to two orthogonal axes can be done by applying the general translational formulae, *Equations 1-3*, and commonly these are applied in strain gauge measurements.

$$\gamma_{xy} = \frac{\varepsilon_d - \varepsilon_c}{\cos \theta_d \sin \theta_d - \cos \theta_c \sin \theta_c}$$

Equation 1

$$\varepsilon_y = \varepsilon_c - \varepsilon_b \cos^2 \theta_c - \frac{\gamma_{xy} \cos \theta_c \sin \theta_c}{\sin^2 \theta_c}$$

Equation 2

$$\varepsilon_x = \varepsilon_b - \varepsilon_y \sin^2 \theta_b - \gamma_{xy} \sin \theta_b \cos \theta_b$$

Equation 3

Using the values of  $\varepsilon_x$ ,  $\varepsilon_y$  and  $\gamma_{xy}$ , Mohr's circle can be constructed and principal values of  $\varepsilon_1$ ,  $\varepsilon_2$  and  $\theta$  evaluated as shown in Figure 8.

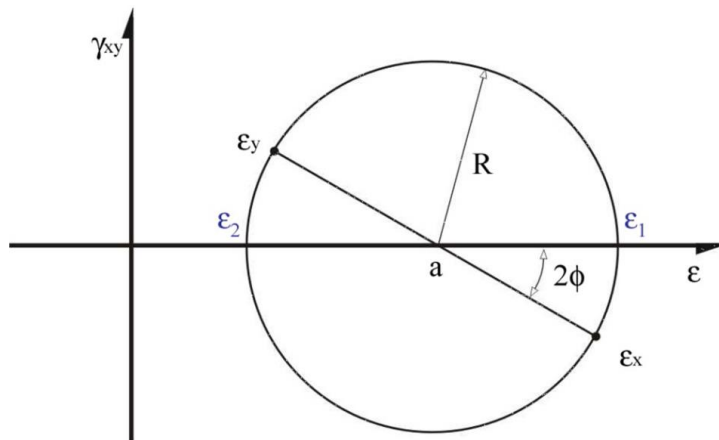


Figure 8. Mohr's circle of strain.

The centre point,  $a$ , and radius,  $R$ , of Mohr's circle can be evaluated as:

$$a = \frac{\varepsilon_x + \varepsilon_y}{2}$$

$$R = \sqrt{\left(\frac{\varepsilon_x - \varepsilon_y}{2}\right)^2 + \left(\frac{\gamma_{xy}}{2}\right)^2}$$

Having evaluated the geometric properties of Mohr's circle, it is relatively simple to determine the principal stresses,  $\varepsilon_1$  and  $\varepsilon_2$ , and the angle between  $\varepsilon_1$  and  $\varepsilon_x$ ,  $\phi$ :

$$\varepsilon_1 = a + R$$

$$\varepsilon_2 = a - R$$

$$\phi = \frac{\text{ArcCos}\left(\frac{\varepsilon_x - a}{R}\right)}{2}$$

By measuring strains at the same point as  $\varepsilon_{b,c,d}$  but perpendicular to the plane they define, i.e. the third principal direction we can complete a full analysis of the strains in three dimensions, these are shown in Figure 9.

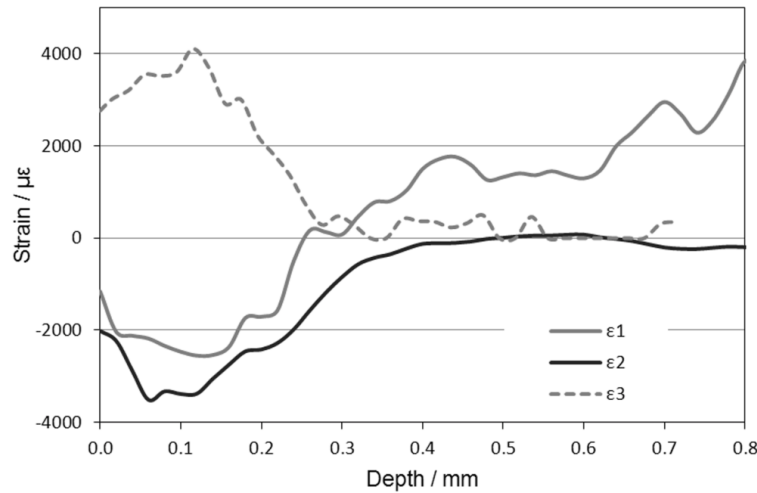


Figure 9. Principal strains evaluated from the measured data in Figure 8.

## 5. TRIAXIAL STRESS DISTRIBUTION

Having obtained the strain in three principal directions it is a straightforward process to evaluate the residual stresses in three dimensions. This is achieved by applying three independent solutions of the general form of Hooke's law, *Equations 4-6*.

$$\sigma_{xx} = \frac{E}{(1+\nu)(1-2\nu)} ((1-\nu)\varepsilon_x + \nu(\varepsilon_y + \varepsilon_z))$$

Equation 4

$$\sigma_{yy} = \frac{E}{(1+\nu)(1-2\nu)} ((1-\nu)\varepsilon_y + \nu(\varepsilon_z + \varepsilon_x))$$

Equation 5

$$\sigma_{zz} = \frac{E}{(1+\nu)(1-2\nu)} ((1-\nu)\varepsilon_z + \nu(\varepsilon_x + \varepsilon_y))$$

Equation 6

where  $E = 73$  GPa is the modulus of elasticity and  $\nu = 0.33$  is Poisson's ratio.

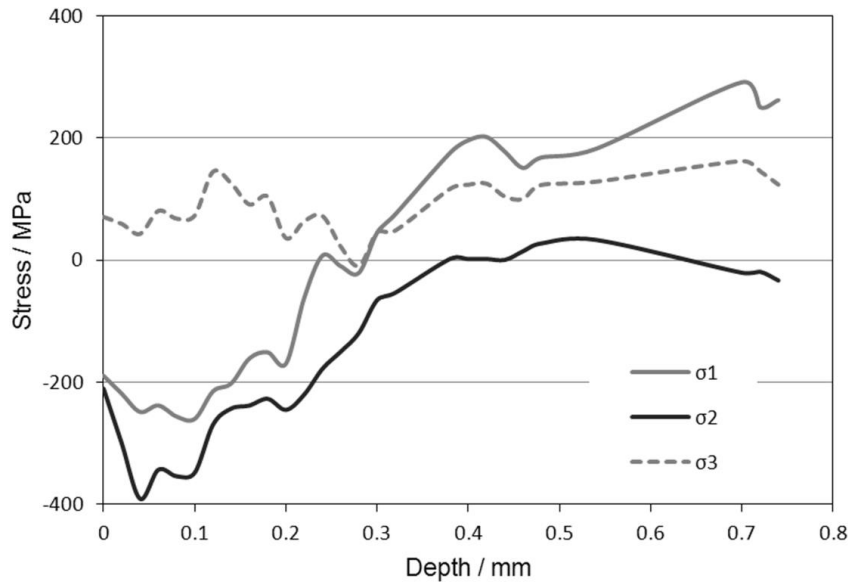


Figure 10. 3D residual stress state evaluated from strains presented in Figure 9.

The data obtained from this type of analysis will be useful in the context of predictive modelling and numerical simulation of materials. The three dimensional residual stress state has been obtained for the strains presented in Figure 9 and is shown in Figure 10.

### 5.1. Comparison with 2D Stress Distribution

Figure 11 shows the 2D stresses produced from the same strain data shown in Figure 7 but assuming a state of plane stress, i.e. omitting the out of plane strains and thereby only considering strains from the planar surface of the specimen. The peak compressive stresses occur at  $\sim 350\text{MPa}$  at a depth of  $100\mu\text{m}$ . The 3D stress plot shows a peak value at  $\sim 400\text{MPa}$ , significantly higher than that shown in 2D. Differences in stress levels can be seen at all depths by comparing the two figures, particularly near the bulk in the 3D plot where  $\sigma_1$  and  $\sigma_2$  differ by  $\sim 400\text{MPa}$ , whereas in the 2D plot the stresses are only  $80\text{MPa}$  apart. Differences on this scale can have a major bearing on predictive models, and whether beneficial or detrimental cannot be overlooked.

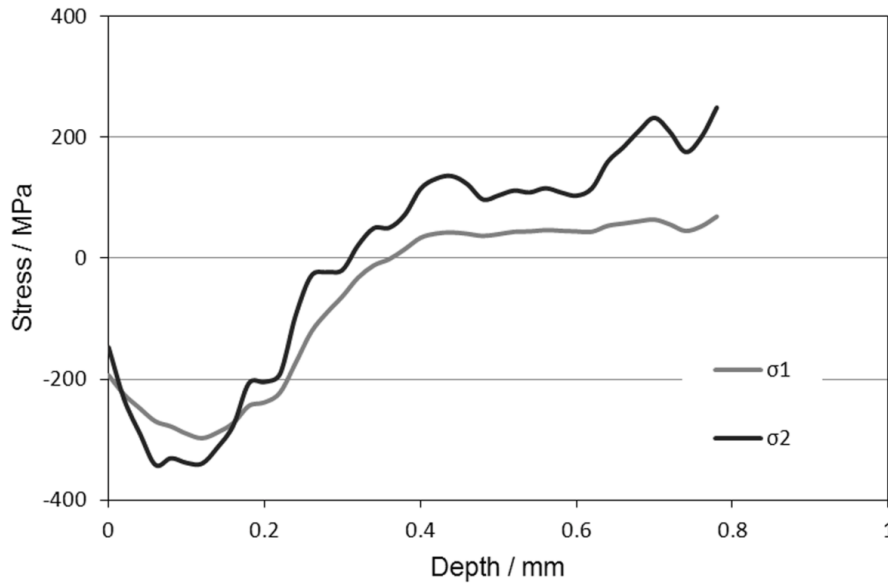


Figure 11. 2D (in-plane) stress distribution produced from the in-plane measured strains.

The curves for 2D principal stresses cross over at  $160\mu\text{m}$ , and this corresponds to an angular shift in the dominant strain direction. By contrast, in Figure 10 the first two principal stress curves ( $\sigma_1$  and  $\sigma_2$ ) do not cross at all suggesting that omitting the third principal strain leads to inaccuracies in angular data, and therefore provides misleading data for analysis and modelling, as subtle changes in the orientations of principal directions can affect the output of

numerical simulations. The desire to increase validity of and, therefore, confidence in simulations requires that experimental data is of the highest possible detail.

The third principal stress ( $\sigma_3$ ) in Figure 10 is often assumed to be negligible in magnitude thereby justifying its omission. It can clearly be seen from this plot that a stress profile exists in this direction and furthermore this stress is tensile. It is widely accepted that tensile stresses are detrimental with regard to the fatigue life. Although loading in the direction of this stress is not typical in most situations, it is probable that occasions will occur where this is not desirable.

## 5.2. Error Analysis

There are several sources of experimental errors in synchrotron diffraction, and some of which can be quantified and incorporated in data presentation. Firstly, it is necessary to consider the influence of user error; problems with mechanical alignment and repeatability are best overcome by rigorous experimental technique and careful use of equipment. Secondly, mechanical errors in the sample translation hardware can result in errors in the diffracted depth, this can be quantified based on manufacturer's specifications for the hardware and incorporated in the depth evaluation.

A more quantifiable amount of uncertainty arises during the fitting process is associated with the confidence in the fitted curve to the raw data obtained. The software used to evaluate spectra in this experiment provides a figure for uncertainty in peak position, as do many peak fitting packages. This can be related directly to an uncertainty in strain and subsequently stress using the relationship between  $\theta$  and  $\epsilon$  by substituting the value for strained peak ( $\theta$ ) centre for its error in peak centre.

$$\epsilon = \frac{\theta - \theta_0}{\tan \theta_0}$$

A further approach to error analysis has been approximated by Chen [12] based on the peak height and is expressed as:

$$U_\epsilon = U_\theta \cot \theta = \frac{U_c \cot \theta}{2} \approx \frac{W \cot \theta}{3\sqrt[3]{C_T}}$$

where:

$U_\theta$  = Error in diffraction angle  $\theta$  (radians)

$U_c$  = Error in peak centre (radians)

$W$  = Peak width at FWHM

$C_T$  = Total number of counts in peak

Errors calculated in such experiments are generally small, of the order of a few percent, and as such difficult to observe on plots unless exaggerated. The most significant but difficult to quantify error is that associated with the evaluation of an unstrained lattice parameter. It is

difficult to be absolute with such a figure, since it varies with the local chemical composition and is therefore heavily dependent on the particular alloy used and also its process history. As such the composition and therefore the crystal lattice vary with position in the material and can provide a more significant source of uncertainty.

## 6. CONCLUSION

A method for measuring the three-dimensional residual stress state has been proposed and demonstrated experimentally. The problems of gauge volume size and specimen orientation relative to the beam were addressed and resolved. Some key considerations arising from this work are that:

- Location of the specimen relative to the beam is critical
- Repeatability in the translation hardware is also important
- Flexibility in the beam slits is important to define different gauge volumes
- Time required to obtain full-field data is large so require a carefully designed experiment.

The differences observed between a 2D and 3D evaluation of the same data suggest that measurement techniques using only in-plane data can be misleading, so care should be taken when using such data to guide simulations.

## ACKNOWLEDGEMENTS

Financial support provided for AY by the UK Engineering and Physical Sciences Research Council (EPSRC) is acknowledged with thanks.

## REFERENCES

- [1] Withers, P. J.; Bhadeshia, H. *Materials Science and Technology*. 2001 17 355–365.
- [2] Withers, P. J.; Bhadeshia H. *Materials Science And Technology*. 2001 17 366–375.
- [3] Lord, J. D.; Grant, P. V.; Fry, A. T.; Kandil, F. A. *Materials Science Forum*. 2002 404-4 567–572.
- [4] Reimers, W.; Pyzalla, A.; Broda, M.; Brusch, G.; Dantz, D.; Schmackers, T.; Liss, K. D.; Tschentscher, T. *J Mater Sci Lett*. 1999 18 581–583.
- [5] Pyzalla, A. *J Nondestruct Eval*. 2000 19 21–31.
- [6] James, M. N.; Hattingh, D. G.; Hughes, D. J.; Wei, L. W.; Patterson, E. A.; Da Fonseca, J. Q. *Fatigue Fract Eng Mater Struct*. 2004 27 609–622.
- [7] Webster, P. J.; Hughes, D. J.; Mills, G.; Vaughan, G. B. M. *Materials Science Forum*. 2002 404-4 767–772.
- [8] James, M. N.; Hughes, D. J.; Chen, Z.; Lombard, H.; Hattingh, D. G.; Asquith, D.; Yates, J. R.; Webster, P. J. *J Eng Fail Anal* 2007 14 384–395.

- 
- [9] Hughes D J, James M N, Hattingh D G and Webster P J 2003 The Use of Combs for Evaluation of Strain-free References for Residual Strain Measurements by Neutron and Synchrotron X-ray Diffraction *Journal of Neutron Research* 11 289–293.
  - [10] Asquith, D. T. *Measurement of 3D residual stresses in shot-peened aluminium alloys*; [MSc-MPhil](#) Thesis. University of Sheffield: Sheffield, UK 2004.
  - [11] Rodopoulos, C. A.; Curtis, S. A.; de los Rios, E. R.; Solis Romero, J. *Int J Fatigue*. 2004 26 849–856.
  - [12] Chen, Z. *Determination of residual stresses using synchrotron x-ray techniques*; MSc Thesis. Salford University: Salford, UK 2001.